Article

Molecular Dynamics Simulations Reveal Octanoylated Hyaluronic Acid Enhances Liposome Stability, Stealth and Targeting

Jingyi Zhu, Limei Xu, Wenxin Wang, Min Xiao, Jian Li, Lushan Wang, and Xukai Jiang*

Cite This: *ACS Omega* 2024, 9, 33833−33844

Read Online

ACCESS | Metrics & More | Article Recommendations | Supporting Information

ABSTRACT: Liposome-based drug delivery systems have been widely used in drug and gene delivery. However, issues such as instability, immune clearance, and poor targeting have significantly limited their clinical utility. Consequently, there is an urgent need for innovative strategies to improve liposome performance. In this study, we explore the interaction mechanisms of hyaluronic acid (HA), a linear anionic polysaccharide composed of repeating disaccharide units of D-glucuronic acid and *N*-acetyl-D-glucosamine connected by alternating β-1,3 and β-1,4 glycosidic linkages, and its octanoylated derivates (OHA) with liposomes using extensive coarse-grained molecular dynamics simulations. The octyl moieties of OHA spontaneously inserted into the phospholipid bilayer of liposomes, leading to their effective coating onto the surface of liposome and enhancing their structural stability. Furthermore, encapsulating liposome with OHA neutralized their surface potential, interfering with the formation of a protein corona known to contribute to liposomal immune clearance. Importantly, the encapsulated OHA maintained its selectivity and therefore targeting ability for CD44, which is often overexpressed in tumor cells. These molecular-scale findings shed light on the interaction mechanisms between HA and liposomes and will be useful for the development of next-generation liposome-based drug delivery systems.
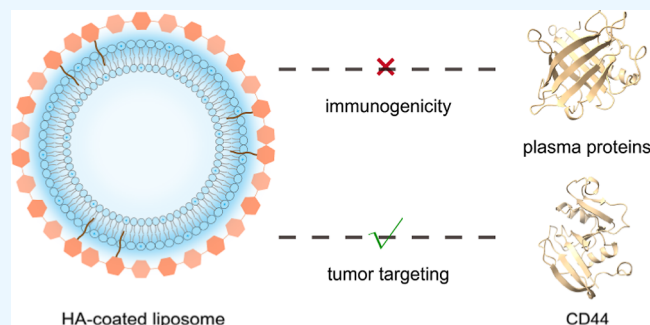
INTRODUCTION

The ease with which liposomes can fuse with cell membranes has resulted in their extensive use in drug delivery.[1] The structural attributes of phospholipid bilayers facilitate the encapsulation, protection, and conveyance of molecules exhibiting diverse physical and chemical properties, including chemotherapeutic drugs, peptides, nucleic acids and ligands.[2,3] Notably, cationic liposomes were successfully developed to combat the COVID-19 pandemic, remarkably reducing infection rates by over 95%.[4] Consequently, liposome-based drug delivery has emerged as a pivotal adjunctive method for drug delivery.[5,6]

Despite the considerable progress made in the utilization of liposomes in biomedicine, substantial challenges in vivo present formidable hurdles for the clinical translation of liposomal drugs.[7] Charrois et al. reported that unstable liposomes could lead to premature release of the encapsulated doxorubicin (DOX), which may result in off-target effects and increased mucocutaneous reactions such as palmar-plantar erythrodysesthesia.[8] Additionally, previous studies revealed that diverse plasma opsonizing proteins, including fibronectin, immunoglobulins, beta 2-glycoprotein, C-reactive protein, and beta 2-macroglobulin, could bind to liposomes and undesirably induced immunological clearance of liposomes.[9] This also limited the clinical application of liposomes for disease treatment. Furthermore, Wilhelm et al. surveyed the literature

within 10 years before 2015 and found the doses of nanoparticles, including liposomes, delivered to solid tumors was only 0.7% (median), implying the lack of selectivity of liposomes for the target site.[10] Collectively, structural stability, immunogenicity and targeting ability are major issues in the clinical use of liposome-based drug delivery systems.[7]

Various materials have been employed to address existing shortcomings and enhance liposomal performance. For example, to improve the stability of nanocarriers by reducing permeability and content outflow, a DNA cross-linked network and derivatives of polyacrylamide hydrochloride have been employed.[11] PEGylation is the most common approach for the development of long-circulating liposomes, although other alternatives including sialic acid, poly(vinyl alcohol), and poly-*N*-vinylpyrrolidones have also been explored for the same purpose.[12] However, these alternatives often show poor selectivity for target site.[13,14] Notably, hyaluronic acid (HA), a linear anionic polysaccharide composed of repeating
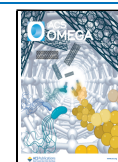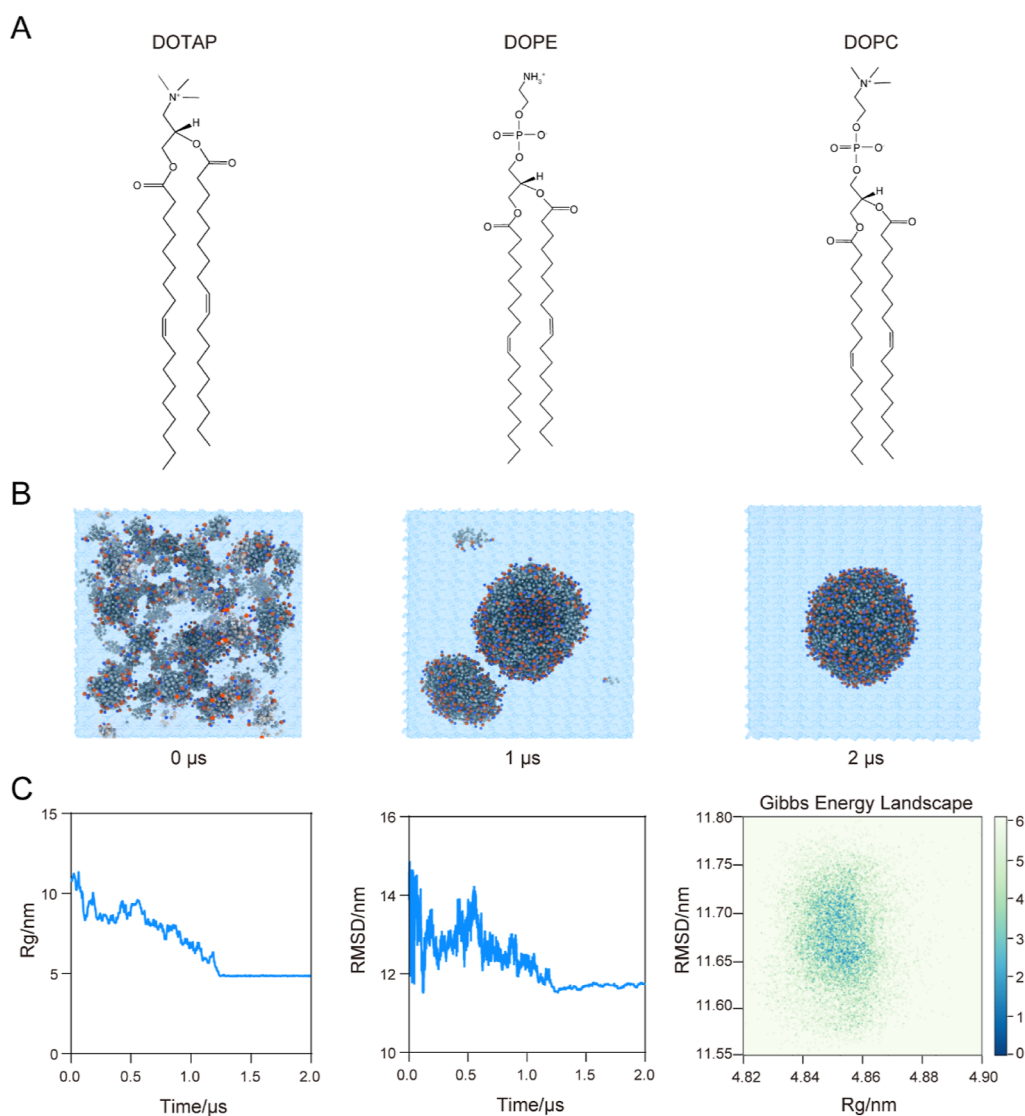
Figure 1. Self-assembly formation of liposome. (A) The structure of lipids used to construct liposomes (LP). (B) Snapshots showing the dynamic process of self-assembly. Hydrocarbon tails are gray, beads containing N are blue, phosphate groups are orange-red, and water molecules are dodger blue. Na$^+$ and Cl$^-$ are omitted for clarity. (C) The radius of gyration (Rg), root-mean-square deviation (rmsd), and Gibbs energy landscape of liposomes.

disaccharide units of D-glucuronic acid (GlcA) and *N*-acetyl-D-glucosamine (GlcNAc) connected by alternating β-1, 3 and β-1, glycosidic linkages, is considered to have substantial potential for innovative drug delivery given it is both nonimmunogenic and specifically targets tumor-rich receptors (e.g., CD44).[15] HA-coated liposomes for targeted delivery of paclitaxel were used to treat breast cancer,[16] while HA-coated liposomal honokiol nanocarriers have been proved to enhance antimetastasis and antitumor efficacy.[17] Although HA is being increasingly used in drug delivery systems for many diseases,[18,19] very little is known about how it interacts with liposomes and the molecular mechanisms underlying the improvements observed in HA-modified liposomal performance.

In the present study, we aimed to examine the potential effects of HA coating on the properties of the liposome using extensive coarse-grained (CG) molecular dynamics simulations, including physiochemical characters, interactions with plasma proteins and CD44. We found that insertion of octyl groups into the phospholipid bilayer promoted HA derivates

coating and stabilized the structural dynamics of liposomes by synergistic effects of electrostatic and hydrophobic interactions. Mechanically, the coating of HA changed the surface electrostatic property of the liposome, inhibiting binding to opsonins associated with immune clearance. Importantly, the unique moieties of HA allowed lipoplexes to target CD44. Taken together, our results elucidate the molecular mechanisms of HA in enhancing liposome performance, with the implications in the design of novel liposome-based drug delivery systems.

■ RESULTS

Phospholipids Self-Assemble into Liposomes. To develop a structural model of liposome, we performed self-assembly MD simulations as described in literature.[20,21] We used CG MD simulations to investigate the self-assembly of liposomes consisting of DOTAP, DOPE and DOPC (mole ratio of 1:2:2) (Figure 1A). Within 2 μs of CG simulations, randomly distributed lipids self-assembled into a liposome (Figure 1B). As shown in Figure S2, scattered lipid molecules
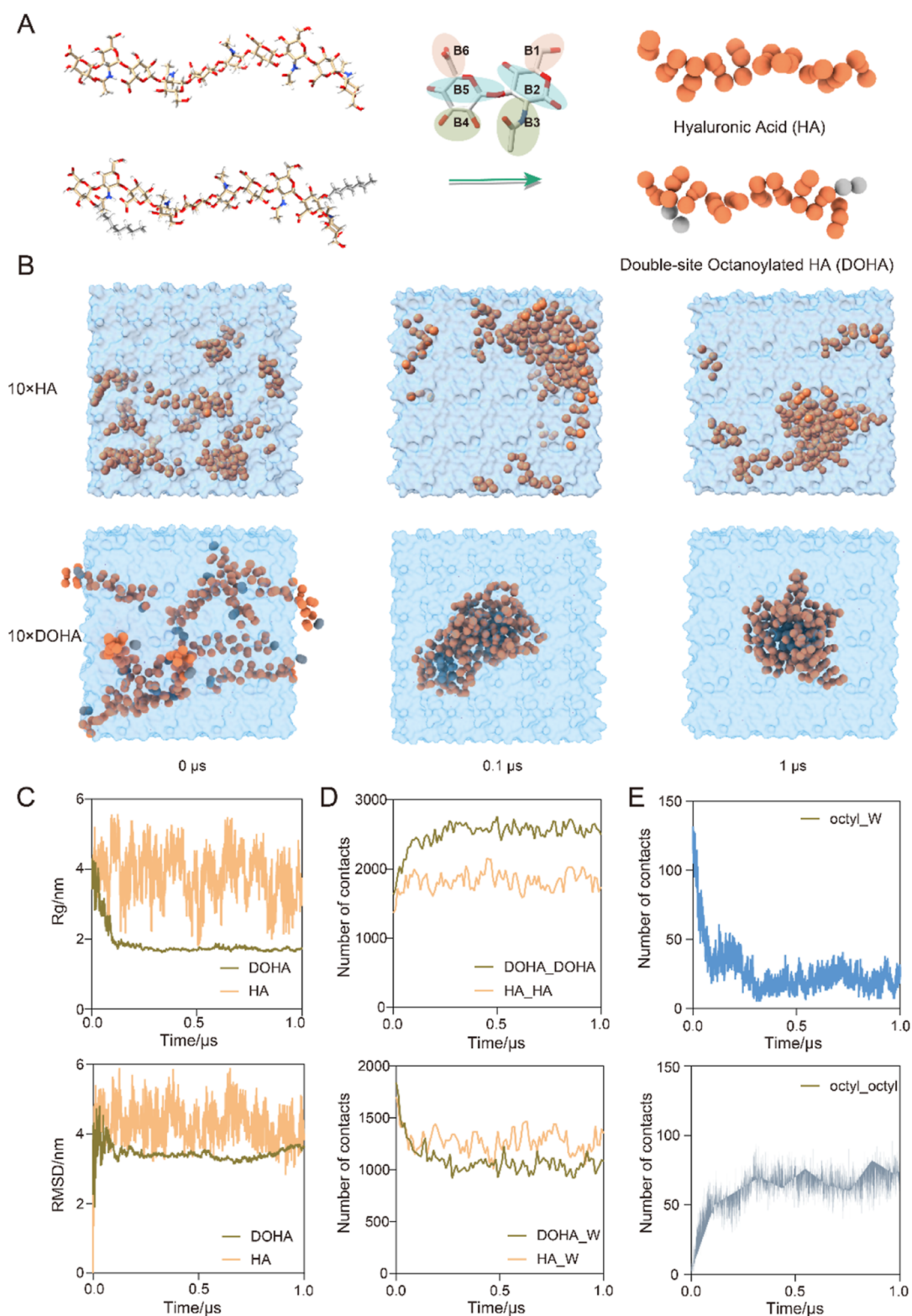
Figure 2. Coarse graining of HA and octanoylated HA. (A) CG models of HA and double-site octanoylated HA (DOHA). The hydrophilic backbone is coral and the octyl groups are gray. (B) Snapshots showing the dynamic behavior of HA and DOHA. (C) The radius of gyration (Rg) and rmsd of HA and DOHA. (D) The interaction of HA or DOHA with each other and water molecules (represented by W). (E) The interaction of the octyl groups on DOHA with each other and water molecules.

first spontaneously aggregate to form multiple small lipid droplets (40 ns). Subsequently, they interacted with each other to form three clusters at 360 ns, and then they merged into two vesicular structures at 920 ns. Eventually, all lipid molecules constituted a complete liposome (1240 ns), which contained a water pocket inside (Figure S3). The diameter of the liposome was approximately 10 nm, which was smaller than that measured experimentally.[22] Such setting was primarily to
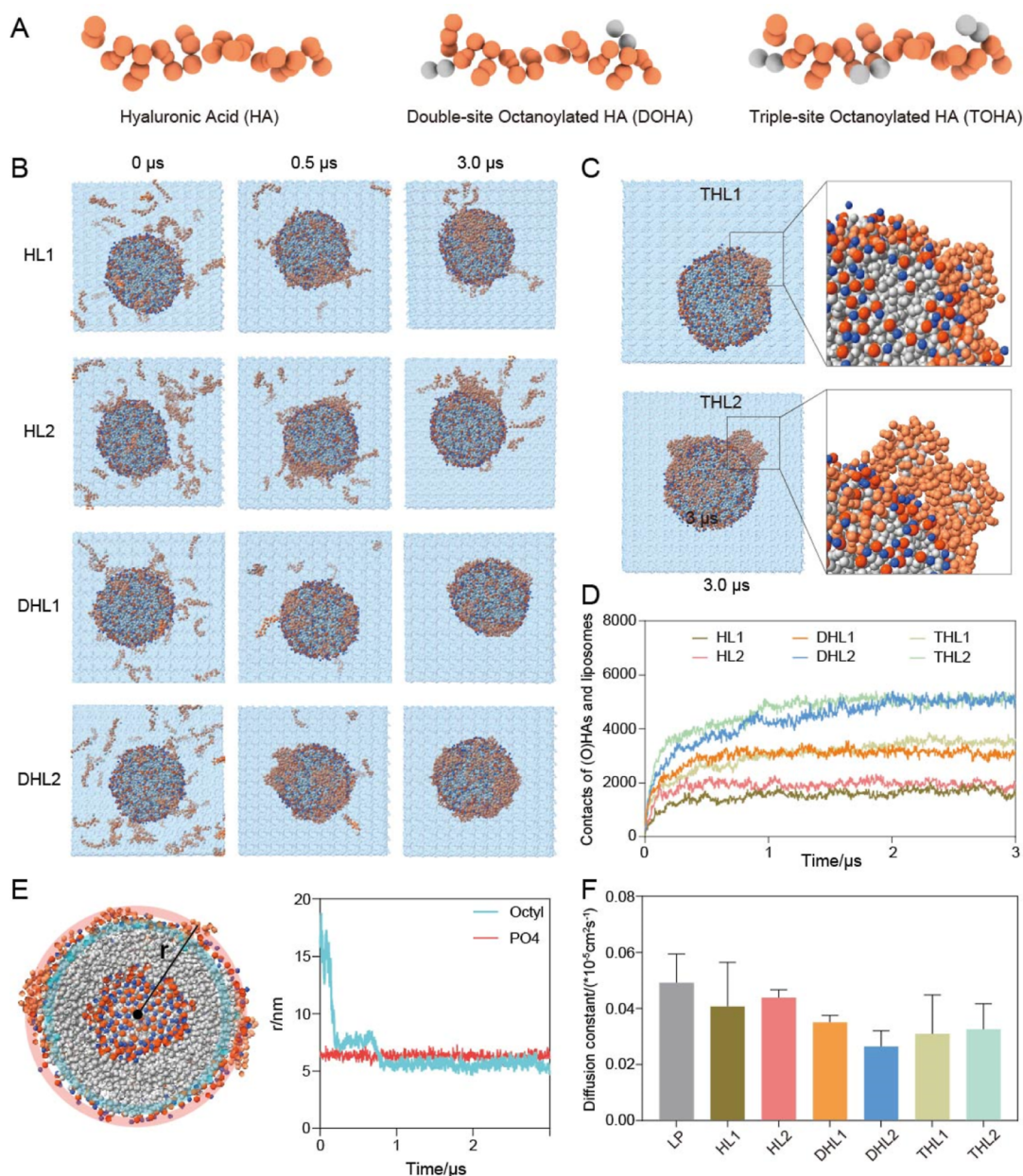
Figure 3. Coating dynamics and the effect on lipoplex stability. (A) Structural models of HA and derivatives with different octanoylated levels. (B) Snapshots showing the coating dynamic process of different lipolexes: HA (HL) and DOHA (DHL)-coated liposomes. TOHA coated liposomes are omitted because of similarity to DHL. The values after the abbreviation, 1 and 2, represent 30 added molecules and 60 add molecules, respectively. (C) The final frames of THLs systems. (D) Number of contacts between various kinds of HA and lipoplexes. (E) The binding mode of octanoylated HA with liposomes and insertion kinetics of a representative octyl groups. Relative positions of liposome surface and octyl groups are indicated by different transparent colors. (F) Diffusion constant of lipids in various lipoplexes, used to measure physical stability.

enhance the simulation sampling. Indeed, small-sized liposomes were often employed in MD simulation studies to observe their structural dynamics in the simulation-accessible time scales.[20,21]

We calculated the radius of gyration (Rg) and rmsd to examine the assembly dynamics (Figure 1C). Both Rg and rmsd displayed a consistent pattern, declining from their initial respective maximum values of 11.83 and 14.98 nm to their minimum values of 4.85 and 11.70 nm over a period of approximately 1.3 μs. This trend suggested the gradual aggregation and fusion of lipids, resulting in the formation of a stable complex. The Gibbs energy landscape generated by Rg and rmsd also indicated that the energy reached the lowest

state near these two minimum values, signifying the completion of self-assembly.

To examine the potential effects of drug encapsulation on the lipid self-assembly process, we conducted new simulations in which 20 DOX molecules were introduced into the system.[23] We found that lipid molecules self-assembled and then formed a liposome after 0.9 μs simulations (Figure S4A), and 10 DOX molecules were encapsulated inside of the liposome (Figure S4B). Further, the radius of gyration of the liposome gradually converged around 4.9 nm, same to the observation in the system without drug molecules. These results indicated that the addition of drug molecules did not affect the lipid self-assembly process. To clarify the computa-

tional model, the drug-free liposome model was used in this study.

Octyl Groups Promote Encapsulation of HA. It has been demonstrated that alkyl modifications could promote the encapsulation of HA.[24] Therefore, we assumed that the alkyl modifications may improve the coating of HA onto the liposome. In addition, Pavan et al. revealed a direct correlation between the length of the alkyl chain and biodegradability.[25] Among different lengths, the octyl groups did not show significant inhibition against hyaluronidases. Therefore, octyl modified HA was employed in the present study. In our preliminary studies using long HA chains, they intended to aggregate by themselves, rather than coated onto the liposome. Moreover, it has been reported that 3−4 disaccharide units of HA are the minimum moiety for the binding to CD44.[26,27] Therefore, we chosen 5 disaccharide units of HA and its octanoylated derivates as the research models (Figure 2A).

The dynamic behavior of HA and DOHA in water was investigated to verify the reliability of model parameters and characterize the effect of hydrophobic alkyl groups. Snapshots showed that HA scattered and distributed randomly, while DOHA self-assembled into spherical nanoparticles (Figure 2B). The Rg and rmsd of HA exhibited fluctuations in the range of 2−6 and 3−6 nm, respectively, whereas those of DOHA rapidly decreased from peak values of 4.12 and 4.75 nm, ultimately converging to the lowest values of 1.98 and 3.62 nm after 0.2 μs (Figure 2C). These data demonstrated the erratic motion of HA in water, whereas DOHA aggregated and became more stable. Furthermore, the number of contacts among HA reached only 1900 but for DOHA exceeded 2700 (Figure 2D), indicating DOHA came into closer contact than HA. Compared to HA, DOHA also had about 500 fewer contacts with the solvent (Figure 2D), indicating a smaller solvent-accessible surface area. Additionally, contacts between octyl groups and water decreased from approximately 130 to ~30, while those among octyl groups increased from 0 to approximately 70 (Figure 2E). These results suggested that octyl groups, serving as the hydrophobic core, promoted the aggregation of the nanoparticle.

HA Coating Stabilizes Structural Dynamics of the Liposome. We prepared both HA and its octanoylated derivatives with varying degrees of substitution to investigate their coating dynamics and influences (Figure 3A). Following 3 μs of CG simulations, only a fraction of the HA interacted with liposomes (HL1 and HL2 systems), while DOHA completely covered the liposomes (DHL1 and DHL2 systems) (Figure 3B). Surprisingly, triple-site octanoylation led to the self-aggregation of some HA derivates into nanoparticles rather than coating liposomes (THL1 and THL2 systems) (Figure 3C). As the concentration of triple-site octanoylated HA (TOHA) increased, the coating effect actually decreased unexpectedly. Thus, TOHA had a weaker ability to shield the surface charge of the liposome compared to DOHA. These findings suggest the existence of an optimal degree of substitution for achieving the desired coating effect.

For the HA-coated liposome systems (HL1 and HL2), the number of contacts of HA with liposomes became saturated at approximately 1800 (HL1) and 2000 (HL2) just before 0.5 μs (Figure 3D), even though the number of HA added in HL2 was twice more than HL1. This phenomenon is likely attributable to electrostatic repulsion resulting from the electronegative nature of HA hindering further binding. However, in DOHA-coated liposome systems (DHL1 and

DHL2), the percent binding rapidly exceeded 87 and 70% within the initial 0.5 μs and reached 100% at 1 and 2 μs, respectively. Consequently, the contact number of DOHA with liposomes eventually exceeded 3000 and 5000, signifying completion of the overall coating process. TOHA exhibited similar coating kinetics to DOHA and a comparable level of coating effect (Figure S5). These findings clearly demonstrate that while octanoylation leads to more efficient and comprehensive binding, higher degrees of substitution do not further enhance the coating effect.

To further investigate the interaction of octanoylated HA with liposomes, we examined the profile of octanoylated HA-coated lipoplex structures (Figure 3E). The backbone of octanoylated HA covered the liposome surface while the octyl groups inserted into the hydrophobic region of membranes. Insertion kinetics showed that the octyl chain started at approximately 15 nm from the mass center of the liposome, moved rapidly and attached to the surface within 0.2 μs, and then inserted into hydrophobic region to a depth of about 1.4 nm by 0.7 μs. The amphiphilic coating mode remained until the end of simulation. These results indicate that the hydrophobic interaction of the alkyl side chain plays a more important role in mediating efficient and complete binding to liposomes than does the electrostatic interaction of the backbone.

To investigate the impact of coating on liposome properties, we determined the diffusion constants of lipids in the seven distinct lipoplexes (Figure 3F). The diffusion coefficient is often used to evaluate the stability of membrane systems, including liposomes.[27−29] All MSD curves were plotted as a function of time on a log−log scale to ensure the validity of extrapolating the diffusion coefficients (Figure S6). The diffusion constant for uncoated lipids (LP system) was 0.049 ± 0.010 ($\times 10^{-5}$ cm^2 s^{-1}). Notably, the diffusion constants of lipids in liposomes coated with 30 and 60 HA molecules (HL1 and HL2) decreased slightly to 0.041 ± 0.0016 and 0.044 ± 0.0029 ($\times 10^{-5}$ cm^2 s^{-1}), respectively, corresponding to about 84 and 90% of lipids in LP. These results show that pure HA could only slightly improve the stability of liposomes. Furthermore, when liposomes were coated with 30 molecules of DOHA (DHL1 system), the diffusion constant of lipids dropped to 0.035 ± 0.0025 ($\times 10^{-5}$ cm^2 s^{-1}), about 71% of lipids in LP. Notably, as the number of DOHA molecules increased to 60 (DHL2 system), the diffusion constant dropped significantly to 0.026 ± 0.0056 ($\times 10^{-5}$ cm^2 s^{-1}), approximately 53% of the diffusion rate observed in the uncoated LP system. These findings indicate that octanoylated HA enhanced the stability of liposomes in comparison to HA, with a positive correlation between the degree of stability enhancement and the number of coatings.

However, as the degree of octanoylation was further increased with TOHA (THL1 and THL2 systems), the diffusion constant did not decrease further but increased to 0.031 ± 0.014 ($\times 10^{-5}$ cm^2 s^{-1}) and 0.032 ± 0.0092 ($\times 10^{-5}$ cm^2 s^{-1}), respectively. These trends aligned with the phenomena illustrated in Figure 3C and suggest the existence of an optimal degree of hydrophobic substitution that maximizes stability enhancement. Although the coating of HA slightly decreased the diffusion of the lipids in the liposome, our results implied the minor role of the coating of HA on the stability of liposome. Under the influence of HA and its derivatives, the liposome radius of gyration remains stable at 4.8 nm (Figure S7A). The membrane thickness of the
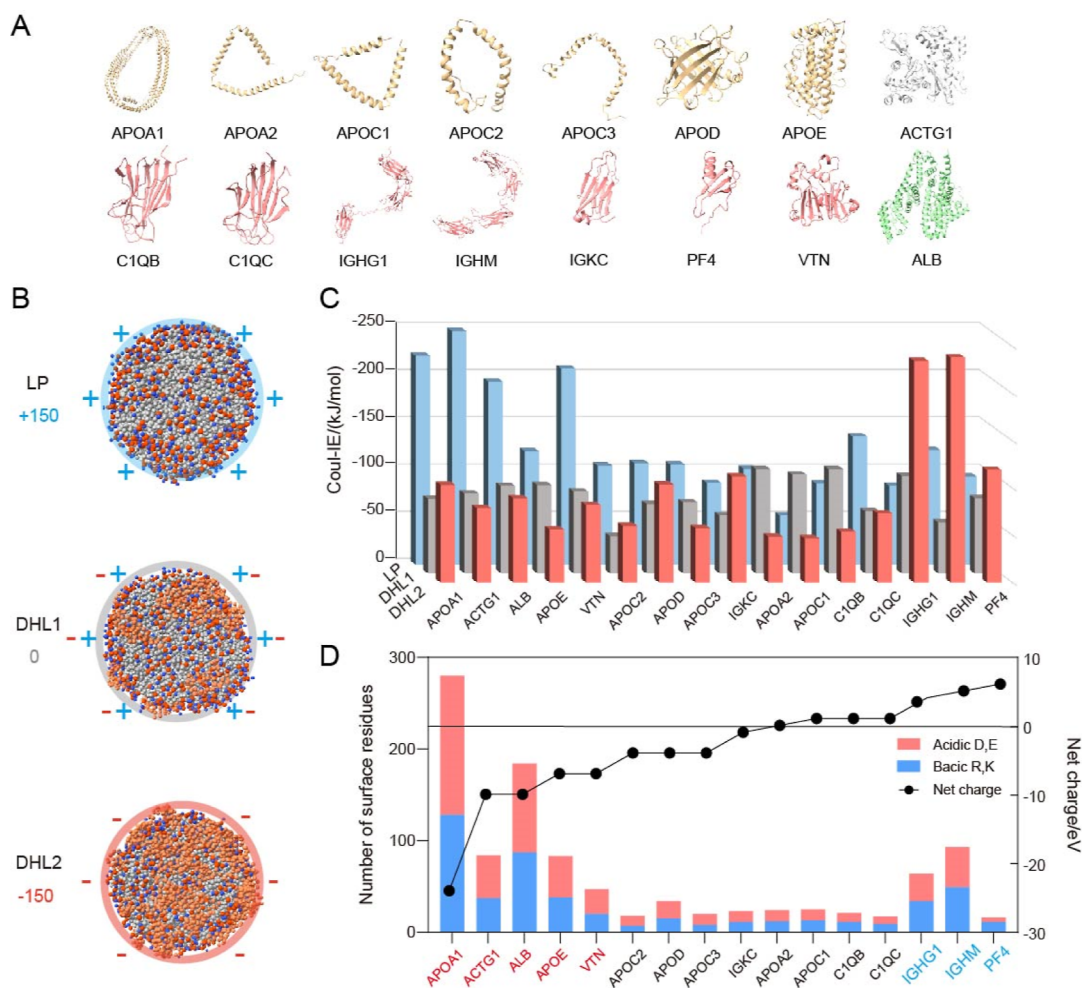
Figure 4. Interactions of human plasma proteins with lipoplexes. (A) Structures of 16 chosen human plasma proteins. (B) Net charge properties of lipoplexes, indicated by different transparent colors. (C) Electrostatic interactions of human plasma proteins with lipoplexes. The colors of pillars correspond to that used in (B). (D) Number of charged amino acids and net charge of proteins surface. The protein names on coordinates have three colors corresponding to the level of net charge. Red means relatively negative and blue means relatively positive. The remaining proteins with relatively neutral net charge are black.

liposome decreased by 0.05 nm (Figure S7B), whereas the area per lipid (APL) increased by ~0.04 nm^2 in the inner leaflet, and ~0.02 nm^2 in the outer leaflet (Figure S7C). These results suggested the structural integrity of the liposomes remained intact when coated with these materials. Given the greatest effects of the DOHA on stability, we selected liposomes coated with DOHA for further investigation.

HA Coating Changes Protein Corona Around the Liposome. Exposure to plasma proteins results in the encapsulation of liposomes by a protein corona, determining their biological identity and fate.[30] We selected 16 plasma proteins for study, consisting of seven apolipoproteins (APOA1, APOA2, APOC1, APOC2, APOC3, APOD, and APOE), actin (ACTG1), platelet factor 4 (PF4), vitronectin (VTN), three immunoglobulins (IGHM, IGHG1, IGKC), two complement proteins (C1QB and C1QC) and albumin (ALB) (Figure 4A).

Electrostatic attraction is an important driving force for protein corona adsorption. To explore the effect of HA on protein corona, we examined electrostatic interactions between three different lipoplexes and each of the selected plasma proteins (Figure 4B,C). In the LP system, APOA1, ACTG1, ALB and VTN exhibited a high degree of affinity, with

electrostatic interaction energies reaching −221.22, −247.18, −193.72 and −207.73 kJ/mol, respectively. In contrast, IGKC (−86.46 kJ/mol), C1QB (−85.66 kJ/mol), and APOC1 (−51.97 kJ/mol) displayed relatively weak affinities to LP. The electrostatic interaction energies of other proteins binding to LP ranged from approximately −100 to −130 kJ/mol. Within the DHL1 system, the highest affinity observed was merely −110.82 kJ/mol for APOA2. APOC1 and C1QB displayed electrostatic interaction energies of −104.80 and −110.78 kJ/mol, respectively. The remaining proteins exhibited moderate binding to DHL1 of about −80 kJ/mol, although APOC2 was only −39.48 kJ/mol. As for DHL2, IGHM and IGHG1 demonstrated the closest attachment to liposomes with electrostatic interaction energies of −238.44 and −234.47 kJ/mol, respectively. APOA2 and APOC1 exhibited weak affinities to DHL2, with electrostatic interaction energies of −48.61 and −46.63 kJ/mol, respectively. These results suggest that coating with HA derivatives can significantly alter the affinity and composition of the protein corona.

We conducted an in-depth characterization of the surface electrostatic properties of the selected proteins (Figures 4D and S8) and analyzed the correlation to binding preference of
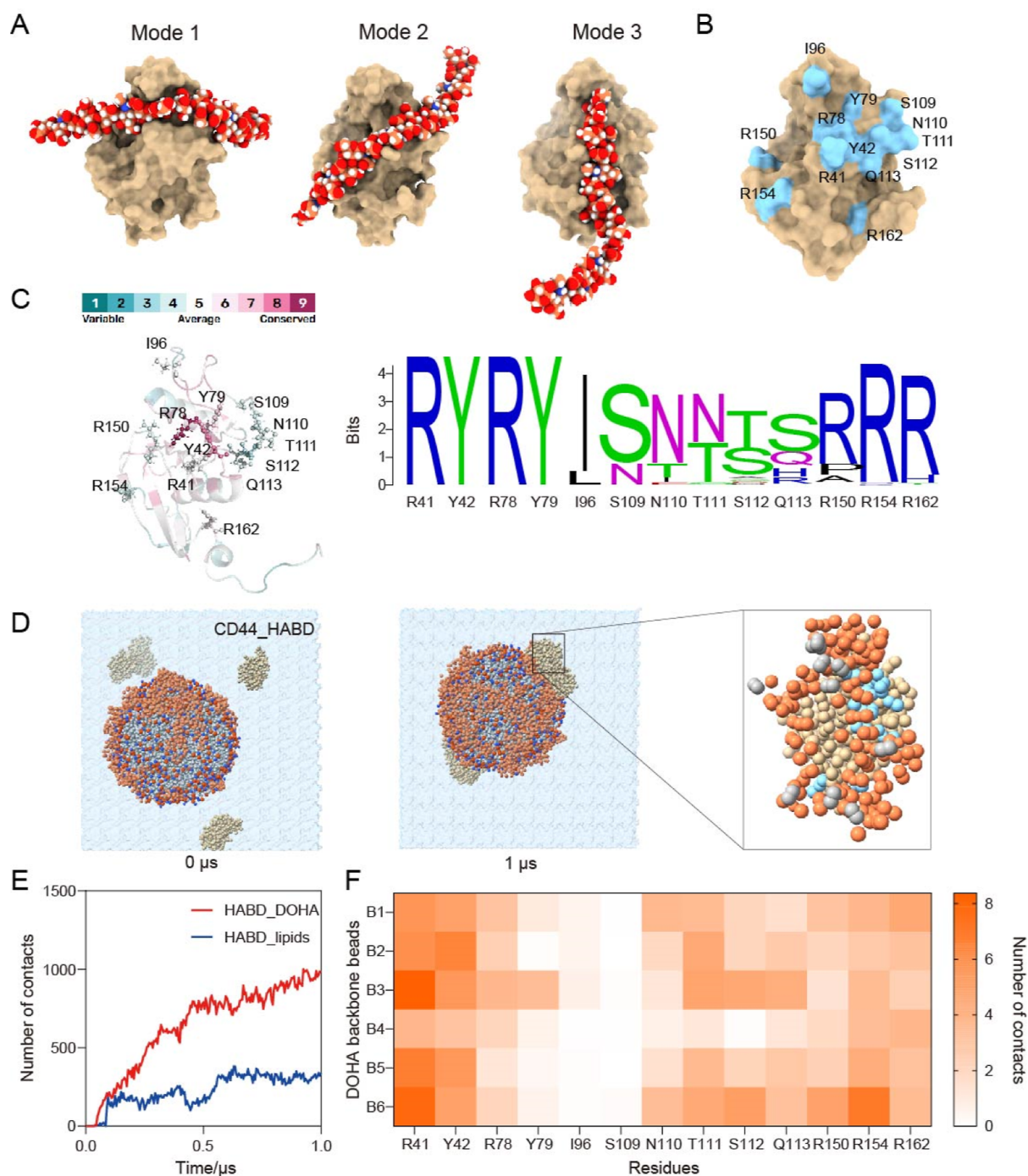
Figure 5. Analysis of lipoplex-CD44 interactions in DHL2. (A) Three different binding modes of HA with the HA binding domain (HABD) of CD44 reported by Vuorio et al. (B) Key residues within the HABD that interact with HA. (C) Conservation analysis and sequence logos of key residues in the HABD. (D) Snapshots showing HABD interactions with lipoplexes and a close-up of the HABD and HA derivates backbone. (E) The number of contacts between HABD with DOHA and lipids, respectively. (F) The number of contacts between DOHA backbone moieties and key residues of the HABD.

various lipoplexes. Notably, the extent of coating directly impacted the overall net charge of the lipoplexes, resulting in a gradient transition from positive to negative charges. Specifically, LP exhibited a net charge of +150 eV, DHL1 was electrically neutral (0 eV), and DHL2 possessed a net charge of −150 eV (Figure 4B). Our findings revealed that positively charged LP preferentially attracted negatively charged proteins such as APOPA1, ACTG1, ALB, APOE and VTN (surface net charges ranged from −24 to −7 eV).

While electrically neutral DHL1 did not exhibit a discernible preference for specific proteins, negatively charged DHL2 preferentially attracted positively charged proteins such as IGHG1, IGHM, and PF4 (surface net charges of +4, +5, and +6 eV, respectively). These results suggest that changes to the protein corona by HA and derivates were mainly achieved by modulation of the surface charge of liposomes.

HA Coating Confers CD44 Targeting on the Liposome. The interaction between HA and CD44 manifests

through three different binding modes (Figure 5A),[27] each associated with particular essential amino acids (summarized in Figure 5B). The analysis of the conservation of these residues (Figure 5C) demonstrated that residues R41, Y42, R78, Y79, R154, and R162 exhibit a high degree of conservation, whereas residues including S109, N110, T111, S112, and Q113 display relatively lower levels of conservation.

We next explored the impact of HA derivates on the CD44 targeting ability of lipoplexes. After 1 μs of CG simulation, the HABD of CD44 bound to the surface of the lipoplex and engaged with the HA derivatives (Figure 5D). Next, we calculated the number of contacts between the HABD and DOHA, as well as membrane lipids (Figure 5E). The number of contacts between the HABD and DOHA continually increased and had reached 1000 by 1.0 μs. In contrast, the number of contacts with membrane lipids remained relatively constant at approximately 350 from 0.6 to 1.0 μs. This observation suggests the HABD interacts with HA derivatives in preference to lipids.

Finally, we examined the interactions between critical residues within the HABD of CD44 and various functional groups of the HA backbone. R41, R150, and R154 predominantly interacted with the electronegative carboxyl groups of the HA backbone with contact numbers of 7.9, 4.8 and 7.0, respectively (Figure 5F). A similar trend was also observed in the DHL1 system (Figure S9). Notably, these amino acids represent conserved sites associated with the crystal and parallel HA binding mode under standard conditions.[27] Consequently, our results suggest that coating on liposomes does not alter HA derivatives binding with CD44, thereby conferring the targeting capacity on liposomes.

■ DISCUSSION

Despite advances in the application of liposomes in biomedicine, few formulations have reached clinical practice.[32,33] This is primarily attributed to the challenges faced by liposomes in vivo, including inadequate stability, susceptibility to phagocytosis, and suboptimal targeting. HA is an important component of the extracellular matrix in connective, epithelial, and neutral tissues of human body, and can be degraded by both reactive oxygen intermediates and hyaluronidases, in particular, HYAL-1 and HYAL-2.[34] Therefore, HA is increasingly used in drug delivery systems for many diseases due to its biocompatibility, biodegradability, and numerous modification sites.[18,19] However, the molecular mechanisms underlying the improvements observed in HA-modified liposomal performance remain insufficiently understood. In the present study, we used long time-scale CG simulations to determine, at the molecular scale, the impact of HA and its derivatives on the properties of liposomes. Furthermore, our study also provides a comprehensive framework for designing innovative lipid-based drug delivery systems.

Liposome stability critically effects therapeutic efficacy. In this study conducted at the molecular level, we investigated the impact of varying degrees of hydrophobic modification of HA on its ability to stabilize liposomes. While electrostatic interactions are often considered the primary driving force for HA coating,[17−19] our results reveal that relying solely on electrostatic adsorption results in incomplete binding. Octanoylation significantly improved coating as insertion of octyl groups into the hydrophobic regions of the lipid bilayer led to additional electrostatic interactions between the HA backbone and polar head groups of phospholipids. This

collaborative action significantly restricted the thermal movement of lipids. However, an excessively high degree of substitution caused alkyl groups to cluster rather than effectively insert into the lipid membrane, leading to coating failure with liposomes. Our findings offer a quantitative mechanistic insight into enhancing the physical stability of liposomes through an amphiphilic binding mode of various HA derivates,[35,36] which is applicable to diverse molecules, including amphiphilic chitosan.[37]

Plasma proteins are a complex and important biosystem compartment which significantly affects the fate of liposomes in vivo.[9] As liposomal interactions with the immune system are associated with immune-related adverse reactions and consequently clinical failure,[38] understanding how liposomes interact with the immune system may help mitigate against these effects. While it has been reported that HA inhibits liposomal clearance by the immune system,[17] the underlying molecular mechanisms remained insufficiently understood. We have demonstrated that HA changes the protein corona associated with liposomes primarily by modulating the liposomal surface charge. Electrically positive liposomes exhibited a discernible preference for negatively charged proteins. For example, APOA1 mediates binding by lymphocytes and phagocytosis by macrophages, and activation of APOE can lead to apolipoprotein receptor-mediated clearance. VTN recruits vitronectin receptors to mediate macrophage phagocytosis.[9] However, the affinity of these proteins for HA-lipoplexes was significantly decreased, which may explain reports of a stealth effect.[36,37] In contrast, excessively negatively charged HA-lipoplex preferentially attract positively charged proteins such as IGHG1, IGHM, and PF4, leading to a shortened half-life.[39,40]

Collectively, our results show that electroneutral HA-lipoplex have the lowest affinity for the selected proteins. Our simulation analysis provides novel mechanistic insights into previously reported experimental observations: macrophage uptake was highest for particles with cationic surfaces, followed by those with anionic surfaces and neutral surfaces.[10] In addition, this study also explained why coating liposomes with negatively charged DNA had the same effect to inhibit opsonin adsorption and substantially reducing accumulation in the spleen and liver.[41] Moreover, there have been investigations involving precoating with plasma proteins to inhibit liposomal clearance.[31] Our findings also provide a theoretical foundation for designing specific adsorption or exclusion characteristics for certain plasma proteins to control the distinct distribution and physiological fate.

Another interesting finding was the mechanism by which HA imparted targeting properties to liposomes. Numerous experimental studies have demonstrated that HA-coated liposomes exhibit superior tumor targeting and accumulation compared to unmodified liposomes.[15,17,18] A prior study reported that HA can engage CD44 through three distinct binding modes (crystal, parallel and upright), each with a unique topographical arrangement.[27] Among these modes were the crystal and parallel binding modes that involved conserved residues R41, R150 and R154, was found to be the most frequently observed. Our findings demonstrate that HA, when bound to liposomes, maintained stable binding to CD44 and adopted the conventional crystal and parallel binding modes. Consequently, our investigation illuminates that HA confers targeting capabilities on liposomes by binding to CD44.

In conclusion, we reported, for the first time, the detailed interaction mechanism of HA and its octanoylated derivates with liposomes. Importantly, we elucidated how such encapsulations modulated the structural properties, protein corona and CD44 targeting of liposomes. These findings provide novel insights into the interaction between biomaterials and liposomes, inspiring further studies on the discovery and design of effective biomaterials for the development of next-generation liposome-based drug delivery systems.

■ MATERIALS AND METHODS

CG Models of Lipids. According to the lipid compositions of cationic liposomes reported in literature,[22,41] three different lipids, namely DOTAP (1,2-dioleoyl-3-trimethylammonium-propane), DOPE (1,2-dioleoyl-sn-glycero-3-phosphoethanol-amine) and DOPC (1,2-dioleoyl-sn-glycero-3-phosphocholine) were used to construct the 3D structure of liposomes using the method of self-assembly MD simulations. The mole ratio of DOTAP/DOPE/DOPC used in our study was 1:2:2. Specifically, 150 DOTAP, 300 DOPC and 300 DOPE (750 lipid molecules in total) were used to construct the liposome. The CG model and parameters of DOPE and DOPC were generated by Martini Maker and Martini 2.2 force field of CHARMM-GUI,[42] while those of DOTAP were generated from the SMILES structural formula through an automatic CG script.[43]

CG Models of HA and Octanoylated Derivates. For the construction of the CG models of HA and octanoylated HA, a mapping scheme reported by Kumar et al. was employed where approximately four heavy atoms were represented by a single CG bead (Figure S1), in accordance with the Martini CG particle building block settings.[44] This mapping strategy was extended to an HA molecule of 10 monosaccharide subunits with 1828 g/mol. The development of DOHA involved octanoylation at the C2-hydroxyl groups of the two GlcA terminals of HA. For the TOHA, an additional octyl group was added to the middle GlcA unit based on DOHA. Each octyl group was composed of 8 carbon atoms and represented by 2 identical C1 beads.

All-atom MD simulations for a single DOHA molecule were conducted for 100 ns under the NPT condition at 310.15 K and 1 bar to calculate the molecular parameters (e.g., bonds, angles and dihedrals), which were mapped and utilized in CG models. The CHARMM36 force field and GROMACS 2021.2 software package were used for these simulations.[45,46] The length of DOHA used here is 4.9 nm, therefore we set the box size of $7 \times 7 \times 7$ nm^3 to allow the DOHA molecule to move freely. Specially, 10 HA and 10 DOHA molecules were solvated separately using CG water particles and neutralized with sodium chloride in an $8 \times 8 \times 8$ nm^3 simulation box and 1 μs production simulations were carried out for each system. Rg and rmsd were used to evaluate structural stability and flexibility. The number of contacts between HA (or DOHA) and water molecules were analyzed to explore their distinct behaviors in water.

CG Models of Proteins. In total, 16 human plasma proteins were used to analyze their interactions with liposomes. Previous studies revealed that these proteins were capable of binding to cationic liposomes.[31,41] All-atom 3D structures of plasma proteins and human CD44 (PDB ID: 1UUH) were obtained from the Protein Data Bank (https://www.rcsb.org/

). Their CG models were developed using the Martini Solution Builder and Martini 2.2 force field in CHARMM-GUI.[47]

Preparation of the Liposome Structure. In the preliminary simulations, we found that the diameter of the liposome was approximately 10 nm. Besides, the diameters of plasma proteins are generally around 5 nm. Considering the periodic boundary conditions, the half-length of the simulation box should be larger than 10 nm to avoid interactions with their own periodic images. Collectively, we therefore constructed the box of $22 \times 22 \times 22$ nm^3 for our simulations. Then, 2 μs production simulations were performed to achieve the self-assembly of liposomes. The radius of gyration (Rg) and rmsd were calculated to examine the self-assembly and structural stability of liposomes. The Gibbs energy landscape that defines the liposome formation was analyzed using the last 200 ns of data for Rg and rmsd. Twenty molecules of DOX were introduced into the self-assembly system to investigate the potential effects of drug encapsulation on the lipid self-assembly process. The CG model and force field parameters of DOX were reported previously.[48]

HA and Octanoylated Derivate-Coated Liposomes. HA, DOHA and TOHA were introduced separately into the simulation system that containing the liposome constructed in Section 2.2. Notably, the charges of complexes were set to have a potential of +150, 0, and −150 eV, by adjusting the number of introduced HA, DOHA and TOHA chains. Table 1 presents

Table 1. Systems and Composition of Molecular Dynamics Simulations[a]

systems	complete designation	key component	potential (eV)
LP	liposome	1 liposome	+150
HL1	HA-coated liposome 1	30 HA + 1 liposome	0
HL2	HA-coated liposome 2	60 HA + 1 liposome	−150
DHL1	DOHA-coated liposome 1	30 DOHA +1 liposome	0
DHL2	DOHA-coated liposome 2	60 DOHA +1 liposome	−150
THL1	TOHA-coated liposome 1	30 TOHA +1 liposome	0
THL2	TOHA-coated liposome 2	60 TOHA +1 liposome	−150

[a]DOHA, DOHA; TOHA, triple-site octanoylated HA.

a summary of the simulation systems: LP (+150 eV), only containing 1 liposome; HL1 (0 eV), containing 30 HA chains and 1 liposome; HL2 (−150 eV), containing 60 HA chains and 1 liposome; DHL1 (0 eV), containing 30 DOHA chains and 1 liposome; DHL2 (−150 eV), containing 60 DOHA chains and 1 liposome; TOHL1 (0 eV), containing 30 TOHA chains and 1 liposome; TOHL2 (−150 eV), containing 60 HA chains and 1 liposome. For each system, 3 μs production simulations were performed to enable the coating processes.

The lipid diffusion constant (D) was calculated to characterize the lipid fluidity in the liposomes based on the following equations

$$\text{MSD} = \langle |r_i(t) - r_i(0)|^2 \rangle \tag{1}$$

$$D = \frac{1}{6 \lim\limits_{t \to \infty} \frac{d}{dt} \sum_{i=1}^{Na} \langle |r_i(t) - r_i(0)|^2 \rangle} \tag{2}$$

where r_i is the displacement of particles and MSD is the average mean square displacement of lipids. D is calculated by

least-squares fitting a straight line ($D \times t + c$) through the MSD(t) (t is time from the reference positions, not simulation time). The membrane thickness and APL of liposomes were also calculated to investigate the effect of encapsulated materials.

Liposome Interaction with Human Plasma Proteins. To investigate the possible binding to liposomes, each of 16 human plasma proteins was introduced into the LP, DHL1, and DHL2 systems, respectively, which generated 48 simulation systems in total. In each system, four copies of the protein were introduced to enhance the sampling. Subsequently, 1 μs production simulations were conducted for each system.

Liposome Interaction with CD44 Hyaluronic Binding Domain. A previous study reported that human CD44 (PDB ID: 1UUH) recognized and bound to HA via three distinct modes.[27] Using human CD44 as the template, 1000 protein sequences were selected by running a blast search in the Uniprot database (https://www.uniprot.org/). MEGA11 was employed for sequence alignment using the ClustalW algorithm.[49] 3D structures obtained from ConSurf (https://consurf.tau.ac.il/) visualized the conservation of CD44. Importantly, sequence profiling of the active site architecture of CD44 was performed by the online software WebLogo (https://weblogo.berkeley.edu/logo.cgi).[50]

To explore the recognition of human CD44 to HA coated liposomes, four copies of hyaluronic binding domain of CD44 (PDB ID: 1UUH) was introduced into the LP, DHL1 and DHL2 systems, respectively. Subsequently, 1 μs production simulations were conducted for each system. The contacts of CD44 with HA derivates and liposomes were analyzed to identify the key residues contributing to their binding.

MD Simulation Parameters. All CG simulations were conducted under periodic boundary conditions using the GROMACS program (version 2021.2) and Martini 2.2 force field.[42,46] To eliminate steric interference, the steepest energy minimization was performed for every system to give the maximum force below 1000 kJ mol^{-1} nm^{-2}. Subsequently, a six-step equilibration cycle was carried out by gradually turning off the position restraints on the lipid and carbohydrate molecules. Finally, production simulations were conducted for each system in the NPT ensemble. To simulate the temperature and pressure inside the human body, the temperature and pressure were coupled to 310.15 K using the velocity rescaling method (time constant of 1 ps)[51] and 1 bar using the isotropic barostat and Parrinello−Rahman algorithm (time constant of 5 ps).[52] The time step was set to 0.02 ps. The simulation interaction cutoff schemes were as follows: van der Waals interactions were smoothly shifted to 0 between 0.0 and 1.1 nm. Coulomb interactions were screened by a relative permittivity constant $\varepsilon_r = 15$ and were shifted to 0 between 0.0 and 1.1 nm. This interaction scheme caused the potential and the forces to vanish at the cutoff. The neighbor list was set to 1.2 nm and updated every 20 steps.

Data Visualization and Statistical Analysis. The structures of lipid molecules were drawn using ChemDraw 18.0. All snapshots extracted from simulated trajectories were displayed with Chimera X.[53] Data were visualized as charts using GraphPad Prism version 9.5.0. and were presented as the means ± standard deviations. Statistical significance was calculated using unpaired Student's t-test by GraphPad Prism 9.5.0 and taken to be ****$p < 0.0001$; ns, not significant.

■ ASSOCIATED CONTENT

ⓢ Supporting Information

The Supporting Information is available free of charge at https://pubs.acs.org/doi/10.1021/acsomega.4c03526.

Figure S1, the CG map of HA disaccharide units; Figure S2, Snapshots of the self-assembly process of lipids; Figure S3, water pocket of the liposome; Figure S4, encapsulation of DOX by self-assembly liposomes; Figure S5, number of contacts between octanoylated HA and liposomes; Figure S6, MSD curves plotted as a function of time on a log−log scale; Figure S7, physiochemical properties of liposomes in different conditions; Figure S8, the surface charge distributions of chosen human plasma proteins; Figure S9, the number of contacts between DOHA backbone moieties and key residues of the HABD in DHL1 (PDF)

■ AUTHOR INFORMATION

Corresponding Author

Xukai Jiang − *State Key Laboratory of Microbial Technology, National Glycoengineering Research Center, Shandong University, Qingdao 266237, China;* ⓞ orcid.org/0000-0002-3624-8732; Email: xukai.jiang@sdu.edu.cn

Authors

Jingyi Zhu − *State Key Laboratory of Microbial Technology, National Glycoengineering Research Center, Shandong University, Qingdao 266237, China;* ⓞ orcid.org/0009-0003-8404-0455

Limei Xu − *State Key Laboratory of Microbial Technology, National Glycoengineering Research Center, Shandong University, Qingdao 266237, China*

Wenxin Wang − *Shandong Institute for Food and Drug Control, Jinan 250000, China*

Min Xiao − *State Key Laboratory of Microbial Technology, National Glycoengineering Research Center, Shandong University, Qingdao 266237, China;* ⓞ orcid.org/0000-0002-4905-8321

Jian Li − *Biomedicine Discovery Institute, Monash University, Melbourne 3800, Australia;* ⓞ orcid.org/0000-0001-7953-8230

Lushan Wang − *State Key Laboratory of Microbial Technology, National Glycoengineering Research Center, Shandong University, Qingdao 266237, China*

Complete contact information is available at:
https://pubs.acs.org/10.1021/acsomega.4c03526

Notes

The authors declare no competing financial interest.

■ REFERENCES

(1) Wang, S.; Chen, Y.; Guo, J.; Huang, Q. Liposomes for tumor targeted therapy: a review. *Int. J. Mol. Sci.* 2023, 24 (3), 2643.

(2) Filipczak, N.; Pan, J. Y.; Yalamarty, S. S. K.; Torchilin, V. P. Recent advancements in liposome technology. *Adv. Drug Delivery Rev.* 2020, 156, 4−22.

(3) Shah, S.; Dhawan, V.; Holm, R.; Nagarsenker, M. S.; Perrie, Y. Liposomes: Advancements and innovation in the manufacturing process. *Adv. Drug Delivery Rev.* 2020, 154−155, 102−122.

(4) Polack, F. P.; Thomas, S. J.; Kitchin, N.; Absalon, J.; Gurtman, A.; Lockhart, S.; Perez, J. L.; Perez Marc, G.; Moreira, E. D.; Zerbini, C.; et al. Safety and efficacy of the BNT162b2 mRNA covid-19 vaccine. *N. Engl. J. Med.* 2020, 383 (27), 2603−2615.

(5) Senapati, S.; Mahanta, A. K.; Kumar, S.; Maiti, P. Controlled drug delivery vehicles for cancer treatment and their performance. *Signal Transduction Targeted Ther.* 2018, 3 (1), 7.

(6) Raj, S.; Khurana, S.; Choudhari, R.; Kesari, K. K.; Kamal, M. A.; Garg, N.; Ruokolainen, J.; Das, B. C.; Kumar, D. Specific targeting cancer cells with nanoparticles and drug delivery in cancer therapy. *Semin. Cancer Biol.* 2021, 69, 166−177.

(7) Tenchov, R.; Bird, R.; Curtze, A. E.; Zhou, Q. Lipid Nanoparticles−From Liposomes to mRNA Vaccine Delivery, a Landscape of Research Diversity and Advancement. *ACS Nano* 2021, 15 (11), 16982−17015.

(8) Charrois, G. J. R.; Allen, T. M. Drug release rate influences the pharmacokinetics, biodistribution, therapeutic activity, and toxicity of pegylated liposomal doxorubicin formulations in murine breast cancer. *Biochim. Biophys. Acta* 2004, 1663 (1−2), 167−177.

(9) Zahednezhad, F.; Saadat, M.; Valizadeh, H.; Zakeri-Milani, P.; Baradaran, B. Liposome and immune system interplay: challenges and potentials. *J. Controlled Release* 2019, 305, 194−209.

(10) Wilhelm, S.; Tavares, A. J.; Dai, Q.; Ohta, S.; Audet, J.; Dvorak, H. F.; Chan, W. Analysis of nanoparticle delivery to tumours. *Nat. Rev. Mater.* 2016, 1 (5), 16014.

(11) Yao, C.; Tang, H.; Wu, W.; Tang, J.; Guo, W.; Luo, D.; Yang, D. Double rolling circle amplification generates physically cross-linked DNA network for stem cell fishing. *J. Am. Chem. Soc.* 2020, 142 (7), 3422−3429.

(12) Prajapati, S. K.; Jain, A.; Jain, A.; Jain, S. Biodegradable polymers and constructs: a novel approach in drug delivery. *Eur. Polym. J.* 2019, 120, 109191.

(13) Gyanani, V.; Haley, J. C.; Goswami, R. Challenges of current anticancer treatment approaches with focus on liposomal drug delivery systems. *Pharmaceuticals* 2021, 14 (9), 835.

(14) Moghassemi, S.; Dadashzadeh, A.; Azevedo, R. B.; Feron, O.; Amorim, C. A. Photodynamic cancer therapy using liposomes as an advanced vesicular photosensitizer delivery system. *J. Controlled Release* 2021, 339, 75−90.

(15) Huang, G.; Huang, H. Hyaluronic acid-based biopharmaceutical delivery and tumor-targeted drug delivery system. *J. Controlled Release* 2018, 278, 122−126.

(16) Ravar, F.; Saadat, E.; Gholami, M.; Dehghankelishadi, P.; Mahdavi, M.; Azami, S.; Dorkoosh, F. A. Hyaluronic acid-coated liposomes for targeted delivery of paclitaxel, in-vitro characterization and in-vivo evaluation. *J. Controlled Release* 2016, 229, 10−22.

(17) Wang, J.; Liu, D.; Guan, S.; Zhu, W.; Fan, L.; Zhang, Q.; Cai, D. Hyaluronic acid-modified liposomal honokiol nanocarrier: enhance anti-metastasis and antitumor efficacy against breast cancer. *Carbohydr. Polym.* 2020, 235, 115981.

(18) Huang, J.; Guo, J.; Dong, Y.; Xiao, H.; Yang, P.; Liu, Y.; Liu, S.; Cheng, S.; Song, J.; Su, Y.; Wang, S. Self-assembled hyaluronic acid-coated nanocomplexes for targeted delivery of curcumin alleviate acute kidney injury. *Int. J. Biol. Macromol.* 2023, 226, 1192−1202.

(19) Pandolfi, L.; Frangipane, V.; Bocca, C.; Marengo, A.; Tarro Genta, E.; Bozzini, S.; Morosini, M.; D'Amato, M.; Vitulo, S.; Monti, M.; et al. Hyaluronic acid-decorated liposomes as innovative targeted delivery system for lung fibrotic cells. *Molecules* 2019, 24 (18), 3291.

(20) Wu, X.; Dai, X.; Liao, Y.; Sheng, M.; Shi, X. Investigation on drug entrapment location in liposomes and transfersomes based on molecular dynamics simulation. *J. Mol. Model.* 2021, 27 (4), 111.

(21) Kesner, L. A.; Piskulich, Z. A.; Cui, Q.; Rosenzweig, Z. Untangling the Interactions between Anionic Polystyrene Nanoparticles and Lipid Membranes Using Laurdan Fluorescence Spectroscopy and Molecular Simulations. *J. Am. Chem. Soc.* 2023, 145 (14), 7962−7973.

(22) Caracciolo, G.; Pozzi, D.; Capriotti, A. L.; Cavaliere, C.; Laganà, A. Effect of DOPE and cholesterol on the protein adsorption onto lipid nanoparticles. *J. Nanopart. Res.* 2013, 15 (3), 1498.

(23) Siani, P.; Donadoni, E.; Ferraro, L.; Re, F.; Di Valentin, C. Molecular dynamics simulations of doxorubicin in sphingomyelin-based lipid membranes. *Biochim. Biophys. Acta Biomembr.* 2022, 1864 (1), 183763.

(24) Hill, T. K.; Abdulahad, A.; Kelkar, S. S.; Marini, F. C.; Long, T. E.; Provenzale, J. M.; Mohs, A. M. Indocyanine green-loaded nanoparticles for image-guided tumor surgery. *Bioconjugate Chem.* 2015, 26 (2), 294−303.

(25) Pavan, M.; Galesso, D.; Secchieri, C.; Guarise, C. Hyaluronic acid alkyl derivative: a novel inhibitor of metalloproteases and hyaluronidases. *Int. J. Biol. Macromol.* 2016, 84, 221−226.

(26) Banerji, S.; Wright, A. J.; Noble, M.; Mahoney, D. J.; Campbell, I. D.; Day, A. J.; Jackson, D. G. Structures of the CD44-hyaluronan complex provide insight into a fundamental carbohydrate-protein interaction. *Nat. Struct. Mol. Biol.* 2007, 14 (3), 234−239.

(27) Vuorio, J.; Vattulainen, I.; Martinez-Seara, H. Atomistic fingerprint of hyaluronan-CD44 binding. *PLoS Comput. Biol.* 2017, 13 (7), No. e1005663.

(28) Wang, Z.; Yan, Y.; Li, C.; Yu, Y.; Cheng, S.; Chen, S.; Zhu, X.; Sun, L.; Tao, W.; Liu, J.; Wang, F. Fluidity-guided assembly of Au@Pt on liposomes as a catalase-powered nanomotor for effective cell uptake in cancer cells and plant leaves. *ACS Nano* 2022, 16 (6), 9019−9030.

(29) Hu, D.; Fumoto, S.; Yoshikawa, N.; Peng, J.; Miyamoto, H.; Tanaka, M.; Nishida, K. Diffusion coefficient of cationic liposomes during lipoplex formation determines transfection efficiency in HepG2 cells. *Int. J. Pharm.* 2023, 637, 122881.

(30) Gibaud, T.; Kaplan, C. N.; Sharma, P.; Zakhary, M. J.; Ward, A.; Oldenbourg, R.; Meyer, R. B.; Kamien, R. D.; Powers, T. R.; Dogic, Z. Achiral symmetry breaking and positive Gaussian modulus lead to scalloped colloidal membranes. *Proc. Natl. Acad. Sci. U.S.A.* 2017, 114 (17), E3376−E3384.

(31) Giulimondi, F.; Digiacomo, L.; Pozzi, D.; Palchetti, S.; Vulpis, E.; Capriotti, A. L.; Chiozzi, R. Z.; Lagana, A.; Amenitsch, H.; Masuelli, L.; et al. Interplay of protein corona and immune cells controls blood residency of liposomes. *Nat. Commun.* 2019, 10 (1), 3686.

(32) Kim, J.; Eygeris, Y.; Gupta, M.; Sahay, G. Self-assembled mRNA vaccines. *Adv. Drug Delivery Rev.* 2021, 170, 83−112.

(33) Akinc, A.; Maier, M. A.; Manoharan, M.; Fitzgerald, K.; Jayaraman, M.; Barros, S.; Ansell, S.; Du, X.; Hope, M. J.; Madden, T. D.; et al. The onpattro story and the clinical translation of nanomedicines containing nucleic acid-based drugs. *Nat. Nanotechnol.* 2019, 14 (12), 1084−1087.

(34) Huang, Y.; Sun, L.; Zhang, R.; Hu, J.; Liu, X.; Jiang, R.; Fan, Q.; Wang, L.; Huang, W. Hyaluronic acid nanoparticles based on a conjugated oligomer photosensitizer: target-specific two-photon imaging, redox-sensitive drug delivery, and synergistic chemo-photodynamic therapy. *ACS Appl. Bio Mater.* 2019, 2 (6), 2421−2434.

(35) Park, J. H.; Cho, H. J.; Yoon, H. Y.; Yoon, I. S.; Ko, S. H.; Shim, J. S.; Cho, J. H.; Park, J. H.; Kim, K.; Kwon, I. C.; Kim, D. D. Hyaluronic acid derivative-coated nanohybrid liposomes for cancer imaging and drug delivery. *J. Controlled Release* 2014, 174, 98−108.

(36) Song, M.; Liang, Y.; Li, K.; Zhang, J.; Zhang, N.; Tian, B.; Han, J. Hyaluronic acid modified liposomes for targeted delivery of doxorubicin and paclitaxel to CD44 overexpressing tumor cells with

improved dual-drugs synergistic effect. *J. Drug Delivery Sci. Technol.* **2019**, *53*, 101179.

(37) Peng, S.; Zou, L.; Liu, W.; Li, Z.; Liu, W.; Hu, X.; Chen, X.; Liu, C. Hybrid liposomes composed of amphiphilic chitosan and phospholipid: preparation, stability and bioavailability as a carrier for curcumin. *Carbohydr. Polym.* **2017**, *156*, 322−332.

(38) Papini, E.; Tavano, R.; Mancin, F. Opsonins and dysopsonins of nanoparticles: facts, concepts, and methodological guidelines. *Front. Immunol.* **2020**, *11*, 567365.

(39) Guan, J.; Shen, Q.; Zhang, Z.; Jiang, Z.; Yang, Y.; Lou, M.; Qian, J.; Lu, W.; Zhan, C. Enhanced immunocompatibility of ligand-targeted liposomes by attenuating natural IgM absorption. *Nat. Commun.* **2018**, *9* (1), 2982.

(40) Palankar, R.; Kohler, T. P.; Krauel, K.; Wesche, J.; Hammerschmidt, S.; Greinacher, A. Platelets kill bacteria by bridging innate and adaptive immunity via platelet factor 4 and FcγRIIA. *J. Thromb. Haemostasis* **2018**, *16* (6), 1187−1197.

(41) Giulimondi, F.; Vulpis, E.; Digiacomo, L.; Giuli, M. V.; Mancusi, A.; Capriotti, A. L.; Lagana, A.; Cerrato, A.; Zenezini Chiozzi, R.; Nicoletti, C.; et al. Opsonin-deficient nucleoproteic corona endows unPEGylated liposomes with stealth properties in vivo. *ACS Nano* **2022**, *16* (2), 2088−2100.

(42) Qi, Y.; Ingolfsson, H. I.; Cheng, X.; Lee, J.; Marrink, S. J.; Im, W. CHARMM-GUI Martini Maker for coarse-grained simulations with the martini force field. *J. Chem. Theory Comput.* **2015**, *11* (9), 4486−4494.

(43) Potter, T. D.; Barrett, E. L.; Miller, M. A. Automated coarse-grained mapping algorithm for the martini force field and benchmarks for membrane-water partitioning. *J. Chem. Theory Comput.* **2021**, *17* (9), 5777−5791.

(44) Kumar, R.; Lee, Y. K.; Jho, Y. S. Martini coarse-grained model of hyaluronic acid for the structural change of its gel in the presence of monovalent and divalent salts. *Int. J. Biol. Macromol.* **2020**, *21* (13), 4602.

(45) Lee, J.; Cheng, X.; Jo, S.; MacKerell, A. D.; Klauda, J. B.; Im, W. CHARMM-GUI input generator for NAMD, GROMACS, AMBER, OpenMM, and CHARMM/OpenMM simulations using the CHARMM36 additive force field. *Biophys. J.* **2016**, *110* (3), 641a.

(46) Van Der Spoel, D.; Lindahl, E.; Hess, B.; Groenhof, G.; Mark, A. E.; Berendsen, H. J. C. GROMACS: fast, flexible, and free. *J. Comput. Chem.* **2005**, *26* (16), 1701−1718.

(47) Qi, Y.; Cheng, X.; Han, W.; Jo, S.; Schulten, K.; Im, W. CHARMM-GUI PACE CG Builder for solution, micelle, and bilayer coarse-grained simulations. *J. Chem. Inf. Model.* **2014**, *54* (3), 1003−1009.

(48) Zhao, L.; Ren, M.; Wang, Y.; An, H.; Sun, F. Delivery mechanism of doxorubicin by PEG-DPPE micelles on membrane invasion by dynamic simulations. *Phys. Chem. Chem. Phys.* **2023**, *25* (23), 16114−16125.

(49) Hall, B. G. Building phylogenetic trees from molecular data with MEGA. *Mol. Biol. Evol.* **2013**, *30* (5), 1229−1235.

(50) Crooks, G. E.; Hon, G.; Chandonia, J.-M.; Brenner, S. E. WebLogo: A Sequence Logo Generator: Figure 1. *Genome Res.* **2004**, *14* (6), 1188−1190.

(51) Bussi, G.; Donadio, D.; Parrinello, M. Canonical sampling through velocity rescaling. *J. Chem. Phys.* **2007**, *126* (1), 014101.

(52) Parrinello, M.; Rahman, A. Polymorphic transitions in single crystals: a new molecular dynamics method. *J. Appl. Phys.* **1981**, *52* (12), 7182−7190.

(53) Pettersen, E. F.; Goddard, T. D.; Huang, C. C.; Meng, E. C.; Couch, G. S.; Croll, T. I.; Morris, J. H.; Ferrin, T. E. UCSF chimeraX: structure visualization for researchers, educators, and developers. *Protein Sci.* **2021**, *30* (1), 70−82.